Inorganic Chemistry
Article

Inorg. Chem. **2009**, *48*, 11399–11406 **11399**
DOI: 10.1021/ic901392q

Photogeneration of Nitrosyl Linkage Isomers in Octahedrally Coordinated Platinum Complexes in the Red Spectral Range

Dominik Schaniel,*,† Theo Woike,† Norwid-R. Behrnd,‡ Jürg Hauser,‡ Karl W. Krämer,‡ Teodora Todorova,¶ and Bernard Delley¶

†*I. Physikalisches Institut, Universität zu Köln, Zülpicherstrasse 77, 50937 Köln, Germany,* ‡*Department of Chemistry and Biochemistry, University of Bern, Freiestr. 3, 3012 Bern, Switzerland, and* ¶*Condensed Matter Theory, Paul Scherrer Institute, 5232 Villigen PSI, Switzerland*

Received July 1, 2009

Octahedrally coordinated platinum nitrosyl complexes $[Pt(NH_3)_4(NO_3)(NO)](NO_3)_2$ (**1**) and $[Pt(NH_3)_4(SO_4)(NO)](HSO_4)(CH_3CN)$ (**2**) undergo linkage isomerization at temperatures below 130 K when excited with red light. Irradiation in the spectral range of 570−800 nm results in an inversion of the NO ligand from a Pt-NO to a Pt-ON configuration. The metastable state Pt-ON can be reverted back to the ground state (GS) Pt-NO by irradiation with blue-green or infrared light or by heating above 130 K. The characteristic shift of the ν(NO) stretching vibration from 1744 to 1815 cm^{-1} in **1** and from 1714 to 1814 cm^{-1} in **2** allowed the unambiguous identification of the respective nitrosyl isomers. Up to 26% of the complexes of **1** and 20% of **2** may be photochemically excited toward the metastable state (MS). Using X-ray crystallography and DFT calculations, it is shown that the Pt-NO in these $\{MNO\}^8$ complexes exhibits a bent arrangement with a Pt−N−O angle in the range of 117−120°. As a consequence and in contrast to the known $\{MNO\}^6$ complexes only one metastable linkage isomer Pt-ON with a correspondingly bent Pt−O−N arrangement is formed, as evidenced by spectroscopy and DFT calculations. The calculated partial density of states shows that the charge transfer transition Pt(5d) → $\pi^\star$(NO) is responsible for the formation of the metastable state.

Introduction

Photochemistry offers the possibility of intramolecular ligand exchange in a controlled and reversible way.[1] Light of a specific wavelength may trigger a linkage isomerization, while light of another energy may restore the initial configuration.[2,3] Complexes exhibiting this photosensitive property are known since Jørgensens and Werners interpretation of the bonding of the NO_2^- ligand in $[Co(NH_3)_5NO_2]Cl_2$, which can be transferred by light from the N-bound to the O-bound Co−ONO configuration.[4−7] A similar behavior was detected in the pale yellow Pt(IV) complex $[Pt(NH_3)_5NO_2]Cl_3$,[8] where the reversible nitro−nitrito isomerization was driven by a chemical reaction. For three decades, the number of complexes known for reversible photoisomerization steadily increases. Such complexes may be described by the general formula $[ML_yZ]^{n\pm}$, where M denotes the central transition metal ion, L coordinating ligands (e.g., Cl^-, NH_3, pyridine), and y their respective multiplicity. Z represents the photosensitive ligand (e.g., N_2, NO^+, NO_2^-, NCS^-, and SO) and n the global charge of the complex.[2,3,9−16] Light irradiation may isomerize up to 100% of the complexes, either in solution or in the solid state, e.g., Ru-NO transforms to Ru-ON,[11] or Ru-SO transforms to Ru-OS in ruthenium sulfoxide compounds.[16] These configurational changes induce novel reactivities. Because the isomeric states are 1−2 eV above the electronic ground state,[17] ligands might

*E-mail: dominik.schaniel@uni-koeln.de.

(1) Kovalevsky, A. Yu.; King, G.; Bagley, K. A.; Coppens, P. *Chem.—Eur. J.* **2005**, *11*, 7254–7264.
(2) Gütlich, P.; Garcia, Y.; Woike, T. *Coord. Chem. Rev.* **2001**, *221*, 839–879.
(3) Coppens, P.; Novozhilova, I.; Kovalevsky, A. *Chem. Rev.* **2002**, *102*, 861–883.
(4) Jørgensen, S. M. *Z. Anorg. Allg. Chem.* **1894**, *5*, 147–196.
(5) Jørgensen, S. M. *Z. Anorg. Allg. Chem.* **1899**, *19*, 109–157.
(6) Werner, A. *Ber. Deut. Chem. Ges.* **1907**, *40*, 765–788.
(7) Adell, B. *Z. Anorg. Allg. Chem.* **1955**, *279*, 219–224.
(8) Basolo, F.; Hammaker, G. S. *Inorg. Chem.* **1962**, *1*, 1–5.
(9) Zöllner, H.; Krasser, W.; Woike, Th.; Haussühl, S. *Chem. Phys. Lett.* **1989**, *161*, 497–501.
(10) Ookubo, K.; Morioka, Y.; Tomizawa, H.; Miki, E. *J. Mol. Struct.* **1996**, *379*, 241–247.
(11) Schaniel, D.; Cormary, B.; Malfant, I.; Valade, L.; Woike, Th.; Delley, B.; Krämer, K. W.; Güdel, H. U. *Phys. Chem. Chem. Phys.* **2007**, *9*, 3717–3724.
(12) Schaniel, D.; Woike, Th.; Delley, B.; Biner, D.; Krämer, K. W.; Güdel, H. U. *Phys. Chem. Chem. Phys.* **2007**, *9*, 5149–5157.
(13) Novozhilova, I. V.; Coppens, P.; Richter-Addo, G. B.; Bagley, K. A. *J. Am. Chem. Soc.* **2006**, *128*, 2093–2104.
(14) Armor, J. N.; Taube, H. *J. Am. Chem. Soc.* **1970**, *92*, 2560–2562.
(15) Schaniel, D.; Woike, Th.; Delley, B.; Boskovic, C.; Güdel, H. U. *Phys. Chem. Chem. Phys.* **2008**, *10*, 5531–5538.
(16) Rack, J. J. *Z. Kristallogr.* **2008**, *223*, 356–362.
(17) Schaniel, D.; Woike, Th.; Delley, B.; Boskovic, C.; Biner, D.; Krämer, K.; Güdel, H. U. *Phys. Chem. Chem. Phys.* **2005**, *7*, 1164–1170.

Published on Web 10/28/2009

be cleaved from the complex. This might be of particular interest for therapeutic applications related to the targeted release of ligands by light irradiation. For an efficient isomerization and release of NO,[18,19] these reactions should be triggered either by red or infrared light because the absorption of tissue and blood in this spectral range is low and light penetration may reach several millimeter depths.

The first photogeneration of nitrosyl linkage isomers in a platinum compound was reported for the octahedral platinumnitrosyl complex $[Pt(NH_3)_4Cl(NO)]Cl_2$.[12] The isomerization of the Pt-NO configuration to the Pt-ON configuration occurs under irradiation in the spectral range of 550−800 nm with a maximum efficiency at 660 nm. At 298 K, the lifetime of the photoinduced isomer in aqueous solution is about 38 μs. In quest of further examples of platinum nitrosyl complexes with this peculiar photosensitivity, two new compounds $[Pt(NH_3)_4(NO_3)(NO)](NO_3)_2$ (**1**) and $[Pt(NH_3)_4(SO_4)(NO)](HSO_4)(CH_3CN)]$ (**2**) were synthesized. Compared to $[Pt(NH_3)Cl(NO)]Cl_2$, the *trans*-to-NO^+ ligand Cl^- was replaced by NO_3^- and SO_4^{2-} and the counterion Cl^- by NO_3^- and HSO_4^-, respectively. Both complexes show photoisomerization of the NO^+ ligand comparable to the original compound. As described below, the change of chemical composition alters the properties of the metastable state. The ground state (GS) and the metastable state (MS) were investigated by differential scanning calorimetry and infrared absorption spectroscopy. In contrast to $[Pt(NH_3)Cl(NO)]Cl_2$ and **1**, where the accuracy of the respective crystal structure suffers from structural disorder, the crystal structure of **2** could be accurately determined. The experimental results are complemented by DFT (density functional theory) calculations on the two cations $[Pt(NH_3)_4(NO_3)(NO)]^{2+}$ and $[Pt(NH_3)_4(SO_4)(NO)]^+$, which allow for an accurate description of the structure of the GS and MS configuration and determination of the corresponding potential surface with energetic minima for GS and MS and activation energies.

Experimental and Computational Details

Synthesis of $[Pt(NH_3)_4(NO_3)(NO)](NO_3)_2$ (1). 1 was prepared from $Pt(NH_3)_4(HCO_3)_2$ (ChemPur GmbH, Germany), conc. HNO_3 (65%, p.a., Merck KGaA, Germany), and NO gas (>95%, Messer Griesheim, Germany). In a sealed glass apparatus, $Pt(NH_3)_4(HCO_3)_2$ (500 mg, 1.3 mmol) was dissolved in 50 mL of degassed, demineralised water under N_2 gas to yield a colorless clear solution. A total of 4 equivalents of HNO_3 (5.2 mmol) were added in portions to convert the bicarbonate into the nitrate salt. The evolving CO_2 was removed by repetitive evacuation and flushing with N_2 gas. After adding NO gas, the solution immediately turned blue, and deep blue crystals precipitated. After 1 day, the crystals were removed from the liquid and dried under N_2 gas. The wet crystals are very sensitive to air. They are rapidly oxidized to Pt(IV) compounds.

Synthesis of $[Pt(NH_3)_4(SO_4)(NO)](HSO_4)(CH_3CN)$ (2). 2 was synthesized from $Pt(NH_3)_4(HCO_3)_2$ (ChemPur GmbH, Germany), conc. sulphuric acid (c = 97%, p.a.; Merck KGaA, Germany), NO gas (>99.5%, Messer Griesheim, Germany), and acetonitrile (HPLC grade, Amtech AG, Switzerland). The acetonitrile was distilled and dried by passing over neutral Al_2O_3.[20]

In a flame-dried vessel, cooled to room temperature under argon, $Pt(NH_3)_4(HCO_3)_2$ (0.102 g, 0.26 mmol) was dissolved in sulphuric acid ($c \approx 8\%$, 5 mL) which was prepared from the conc. acid by dilution with deaerated demineralized water. After gas evolution had ceased, the colorless solution was carefully degassed under vacuum and purged with argon (five cycles). Addition of NO gas resulted in a deep blue solution, which was allowed to stay for 3 h unstirred at room temperature. Acetonitrile (3 mL) was carefully added by canulation to form a layer on top of the solution. Keeping a slight over pressure of NO gas, the addition of acetonitrile was repeated three times each 24 h, using the same volume, until the fourth day, blue crystals precipitated and the solution became pale blue. Under argon, the vessel was opened, and the supernatant liquor was rapidly removed with a Pasteur pipet. Still under argon, droplets of the solution attached to the surfaces of the crystals were rapidly and carefully removed with soft filter paper before placing the sample under paraffin oil. Isolated: 0.051 g (0.10 mmol, 38%) of deep blue prismatic crystals. Wet crystals of **2** rapidly decompose in air to a white powder. Trials to increase the yield by further addition of acetonitrile combined with longer crystallization times led to the decomposition of the previously formed blue crystals into a white precipitate not further investigated.

X-ray Structure Determination. Samples were kept immersed in paraffin oil. Suitable single crystals for X-ray diffraction analysis were selected under a microscope, rapidly transferred to a Nylon loop filled with Paratone N (HR2-643, Hampton Research, U.S.A.), and frozen during mounting on the diffractometer.

Single crystal diffraction data were collected on a Bruker APEX II diffractometer.[21] After empirical absorption correction with Sadabs,[22] the crystal structure was solved with SHELX on F_o^2 and refined with SHELXL[23] against F_c^2. All H atoms were introduced on geometrically calculated positions and refined using a riding model and optimizing the free torsion angle to maximize the electron density at the hydrogen positions. The isotropic displacement parameters of the H atoms were assigned to a value equal to 1.5 U_{eq} of their parent C, N, or O atoms. For all non-H atoms, anisotropic temperature factors were refined. Structural figures were prepared with Diamond3.[24]

DSC Measurements. Differential scanning calorimetry (DSC) measurements were done on a Mettler DSC 30 equipped with quartz windows in the cryostat for illumination. For the population of the metastable state, the powder in an Al crucible was irradiated by unpolarized light of a metal halide lamp (Osram HMI-575 W), narrowed by a set of interference filters at 586 and 710 nm (fwhm = 7 nm) or by the monochromatic

(18) Eroy-Reveles, A. A.; Leung, Y.; Beavers, C. M.; Olmstead, M. M.; Mascharak, P. K. *J. Am. Chem. Soc.* **2008**, *130*, 4447–4458.
(19) Rose, M. J.; Mascharak, P. K. *Curr. Op. Chem. Biol.* **2008**, *12*, 238–244.
(20) Pangborn, A. B.; Giadello, M. A.; Grubbs, R. H.; Rosen, R. K.; Timmers, F. J. *Organometallics* **1996**, *15*, 1518–1520.

(21) Single crystal diffraction data were recorded on a Bruker Apex II CCD diffractometer at 173(2) K employing Mo Kα radiation (λ = 0.71073 Å, graphite monochromator). Crystal data: molecular formula, $C_2H_{15}N_6O_9PtS_2$; molecular weight, 526.41 g/mol; crystal system, monoclinic; space group, $P2_1/c$ (No. 14), a = 7.7441(3) Å, b = 19.2289(6) Å, c = 9.5902(3) Å, β = 91.6590(10)°, V = 1427.48(8) Å^3, Z = 4, ρ = 2.454 g/cm^3 (calculated), μ = 10.17 mm^{-1}, $F(000)$ = 1008; crystal size, 0.32 × 0.29 × 0.19 mm. Data collection: $2.12 \le \theta \le 40.25°$; index range, $-14 \le h \le 14$, $-34 \le k \le 32$, $-17 \le l \le 17$. Observed reflections: 73967, unique reflections, 8962; observed reflections with $I > 2\sigma(I)$, 8317; R_{int} = 0.0354. Model data: $R1[I > 2\sigma(I)]$ = 0.0232, $R1$(all data) = 0.0259, $wR2$(all data) = 0.0552 with $w = 1/[\sum F_o^2 + (0.0220P)^2 + 1.7405P]$, where $P = (F_o^2 + 2F_c^2)/3$. Residual electron density ρ (min) = −2.891 eÅ^{-3}, ρ (max) = 3.004 eÅ^{-3}. Goodness of fit S: 1.153. CCDC-740489 contains supplementary crystallographic data for this paper. These data can be obtained free of charge from The Cambridge Crystallographic Data Centre via www.ccdc.ac.uk/data request/cif.

(22) *Sadabs*. Bruker AXS, Inc.: Madison, Wisconsin.
(23) Sheldrick, G. M. *SHELX and SHELXL-97: Programs for Solution of Crystal structures*. University of Göttingen: Germany (1997).
(24) *Diamond3*, Crystal Impact GbR: Bonn, Germany.

light of diode lasers (635, 660, 685, 785, and 850 nm). Very rapid depopulation of the metastable state MS was achieved by laser irradiation at 532 or 1064 nm. The light exposure $Q = \int I(t)\mathrm{d}t$ on the sample is given by the integral over the product of light intensity I and irradiation time t. The dynamic measurements were performed with a linear heating rate of $q = \mathrm{d}T/\mathrm{d}t = 4$ K/min. The corresponding spectrum of the unirradiated sample was subtracted to obtain a horizontal baseline in the temperature range of the thermal decay. The detected signal of the DSC (heat flow) is the time derivative of the enthalpy $\mathrm{d}H/\mathrm{d}t$ over the temperature. The total enthalpy of the decay is then given by integration over time or temperature. The activation energy E_A and the frequency factor Z of the Arrhenius-like decay are obtained by fitting the measured data to the equation

$$\frac{\mathrm{d}H(T)}{\mathrm{d}t} = H_{\mathrm{tot}} Z \times \exp\left(-\frac{E_A}{k_B T} - \frac{Z}{q}\int_{T_0}^{T} \exp\left(-\frac{E_A}{k_B T'}\right)\mathrm{d}T'\right) \quad (1)$$

where k_B denotes the Boltzmann constant, q the heating rate, and T_0 is the starting temperature for the integration. The integration is performed numerically over the temperature range of the decay. The total decay enthalpy H_{tot} is proportional to the population P of the MS which depends on the light exposure Q. H_{tot} is modeled by eq 2.

$$H_{\mathrm{tot}} = H_{\mathrm{sat}}[1 - \exp(-Q/Q_0)] \quad (2)$$

The MS were populated by light irradiation at 90 K in a N_2 atmosphere. Further details concerning the evaluation of the DSC data are given in ref 17.

Infrared Absorption Spectra. Infrared absorption spectra were measured with a Nicolet 5700 FTIR spectrometer. Sample preparation was difficult because of the reaction of the present platinum complexes with KBr and CsI, which results in a color change from gray-blue to black. Thus, finely ground samples were embedded in Nujol and subsequently deposited on a CsI pellet. This pellet was mounted on a copper coldfinger with silver paste ensuring good thermal contact. The sample was then cooled to 80 K in a liquid nitrogen cryostat equipped with CsI windows. Samples of $[Pt(NH_3)_4Cl(NO)]Cl_2$, prepared and measured in the same manner, served as reference. Furthermore pellets with AgBr were prepared, which showed no color change of the platinum complexes. The population of the metastable state was derived from the decrease of the integral of the absorption band of the ground state ν(NO) stretching vibration.

DFT Calculations. Density functional theory (DFT) calculations were performed for the cations $[Pt(NH_3)_4(SO_4)(NO)]^+$ and $[Pt(NH_3)_4(NO_3)(NO)]^{2+}$, using the all electron density functional theory DMol^3 code.[25,26] A double numerical polarized (DNP) basis set, which includes all occupied atomic orbitals plus a second set of valence orbitals plus polarized d valence orbitals, is employed. Perdew−Burke−Ernzerhof (PBE)[27] exchange−correlation potential and density functional semicore pseudopotential (DSPP)[28] with scalar relativistic corrections to atomic scattering properties are used. The following geometry optimization convergence thresholds were used (a.u.): 0.0001 (energy change), 0.001 (maximum force), and 0.01 (maximum displacement). Beside the interatomic distances and angles in the cation, the vibrational frequencies in GS and MS, as well as the potential energy over the reaction coordinate from GS to MS were calculated, and the partial density of states (pDOS) of Pt, N, and O were calculated for a clear assignment of the optical transitions. Information on the distribution of molecular levels and their orbital characters is shown graphically in analogy to partial density of states figures in solid-state studies. The discrete molecular levels are shown as a histogram, and Mulliken population gives the histogram heights.

The DMol^3 is a method[25,28] for DFT calculations of molecular clusters in the gas phase. It is generalized[29] to model a solvent environment of a molecule via the conductor-like screening model (COSMO).[30] This method involves the construction of a solvent accessible surface (SAS) and solution of electrostatics. The SAS is defined via element dependent radii, with values typically about 17% larger than the van der Waals radii. The SAS is a model of a surface where the induced charges are located. The detailed construction is discussed in a previous publication.[31]

Table 1. Selected Crystallographic Data of **1** and **2**

compound	**1**	**2**
empirical formula	$N_8H_{12}O_{10}Pt$	$C_2H_{16}N_6O_9PtS_2$
formula weight (g/mol)	479.24	527.41
T/K	173(2)	173(2)
space group	*I*4/*mmm* (no. 139)	$P2_1/c$ (no. 14)
a (Å)	7.6609(10)	7.7441(3)
b (Å)		19.2289(2)
c (Å)	9.7911(15)	9.5902(3)
β (deg)		91.659(1)
cell volume (Å^3)	574.6(1)	1427.48(8)
Z	2	4
calc. density/g/cm^3	2.773	2.454
R indices, $I > 2\sigma(I)$	R1 = 2.8%, wR2 = 6.5%	R1 = 2.3%, wR2 = 5.4%
R indices, all data	R1 = 3.3%, wR2 = 6.9%	R1 = 2.6%, wR2 = 5.5%

Results

Crystal Structure of $[Pt(NH_3)_4(NO_3)(NO)](NO_3)_2$ (1). The crystal structure of **1** was solved from X-ray diffraction data. It is composed of the complex cation $[Pt(NH_3)_4(NO_3)(NO)]^{2+}$ and nitrate counteranions. Crystallographic data are summarized in Table 1. The octahedral Pt complex has four equatorial ammonia ligands, an O-bond axial NO_3 ligand, and an axial NO ligand in bent configuration as described for **2** below. The central Pt ion of the complex is located on site (2b) with site symmetry 4/*mmm* of the tetragonal space group *I*4/*mmm*. However, the ligands cannot adopt such a high symmetry of the complex, and the structure shows various degrees of disorder. The ammonia ligands have a rotational disorder around the Pt−N bonds. The axial nitrate ligand has a 2-fold disorder with respect to the 4/*m* axis. The axial nitrosyl ligand shows a 4-fold disorder of the O atom with respect to the Pt−N bond. Furthermore, the axial nitrate and nitrosyl ligands show an upside-down disorder. Such obstacles prohibited a high precision structure determination, and we restrict ourselves to a qualitative account on **1** only. In contrast, a high precision structure determination was possible for **2**, see below.

(25) Delley, B. *J. Chem. Phys.* **1990**, *92*, 508–517.
(26) Delley, B. *Phys. Rev. B* **2002**, *66*, 155125.
(27) Perdew, J. P.; Burke, K.; Erznerhof, M. *Phys. Rev. Lett.* **1996**, *77*, 3865–3868.
(28) Delley, B. *J. Chem. Phys.* **2000**, *113*, 7756–7764.
(29) Andzelm, J.; Kölmel, Ch.; Klamt, A. *J. Chem. Phys.* **1995**, *103*, 9312–9320.
(30) Klamt, A.; Schüürmann, G. *J. Chem. Soc. Perkin Trans. 2* **1993**, 799–805.
(31) Delley, B. *Mol. Sim.* **2006**, *32*, 117–123.

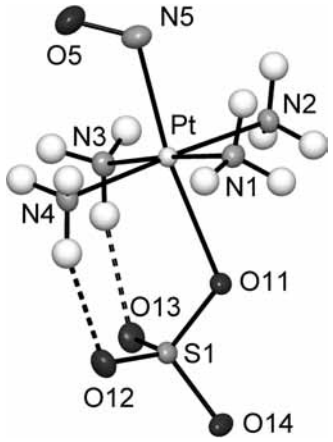

Figure 1. $[Pt(NH_3)_4(SO_4)(NO)]^+$ complex of **2**. Atoms are shown as 50% probability ellipsoids.

Crystal Structure of $[Pt(NH_3)_4(SO_4)(NO)](HSO_4)(CH_3CN)$ (2). The structure of **2** is composed from the complex cations $[Pt(NH_3)_4(SO_4)(NO)]^+$, HSO_4^- anions, and acetonitrile solvate molecules. The monoclinic unit cell, space group $P2_1/c$, contains four formula units, and all atoms occupy the common site (4e). Crystallographic data are summarized in Table 1 and important distances and angles in Table 2. The nitrosyl complex is shown in Figure 1. It consists of the central Pt ion, four equatorial ammonia ligands, an axial oxo ligand from a sulfate group, and the nitrosyl ligand NO *trans* to it. The nitrosyl ligand has a bent configuration with respect to Pt as expected for a d^8-NO complex.[32] A few examples of bent Pt−N−O configurations for octahedrally coordinated Pt-complexes have been described earlier.[33,34] The atomic distances are Pt−N5 2.081(2) Å and N5−O5 1.133(3) Å with a Pt−N5−O5 angle of 117.4(2)° (Figure 1 and Table 2). The Pt-NH_3 coordination is close to square planar. The Pt−N distances of the equatorial ammonia ligands are within the narrow range of 2.054−2.061 Å. Their *cis* N−Pt−N angles deviate less than 1° from 90°. Pt is located 0.0464(8) Å toward NO with respect to the best plane defined by the four N atoms of the ammonia ligands. Both *trans* N−Pt−N angles of the ammonia ligands are close to 177.25(6)°. The S1 sulfate group is connected to the complex via O11. Its geometry slightly deviates from a tetrahedron as it shows two shorter and two longer S−O bonds of an average 1.4623 Å and 1.4936 Å, respectively (Table 2). Five of the O−S−O angles are within 109.79−110.67°, close to the tetrahedral angle of 109.47°. The O11−S−O14 angle of 105.41(8)° is significantly smaller. The distortion of the S1 sulfate group results from its coordination to the complex. The S1−O11 bond with 1.496(1) Å is longer because O11 is bound to Pt at a distance of 2.284(1) Å. Two O atoms of the sulfate group form intra complex H-bonds with the N3 and N4 ammonia ligands, i.e., N4−H4C···O12 and N3−H3C···O13. Further H-bonds link the complexes and the HSO_4^- anions to a three-dimensional structural network (Figure 2). The H-bonds N1−H1A···O12, N2−H2C···O13, N3−H3B···O14, and N4−H4C···O12 with N−O distances between 2.85−3.00 Å connect the complexes to chains along the *c*-axis. Those chains are further connected by the HSO_4^- anions. First, they are linked to the sulfate group by the O23−H23··· O14 H-bond with a short O−O distance of 2.569(2) Å. Then, they form further H-bonds to ammonia ligands, i.e., N1−H1C···O24, N2−H2A···O21, N3−H3A···O22, and N4−H4B···O22. The later two link the chains along the *a*-axis. The HSO_4^- anions around S2 are characterized by a long S2−O23 bond of 1.545(2) Å that clearly indicates the presence of the H atom H23, which was also directly visible in the difference Fourier map of the electron density at this position. The other S2−O bonds range from 1.444−1.469 Å. The H-bond network results in channels along the *c*-axis located at $\frac{1}{4}$, $\frac{1}{4}$, *z* and $\frac{3}{4}$, $\frac{3}{4}$, *z* which are occupied by the acetonitrile molecules. Their CH_3 group points toward the NO ligand, and the N11−C11−C12 axis is almost parallel to the N5−Pt−O11 axis.

As shown on the example of $[Ru(py)_4Cl(NO)][PF_6]_2 \times \frac{1}{2}H_2O$, the structure of GS and MS in ML_5NO complexes can be calculated with high accuracy by DFT.[35,36] Therefore, we calculated the structure of the two platinum nitrosyl complexes in GS and MS. The results are shown in Figure 3. Comparison of the calculated GS structure of $[Pt(NH_3)_4(SO_4)(NO)]^+$ with the measured one of **2** (Table 2) shows that the largest differences are found for the equatorial Pt−N distances of the order of 0.04 Å and in the SO bonds of the SO_4^{2-} group up to 0.06 Å. The calculated H positions of the N1 and N2 ammonia ligands differ from the experimental ones with respect to the rotation about the Pt−N bond. This is intuitively clear because the intermolecular H-bonds are not accounted for by the calculation on the free cation. The calculated bond lengths Pt−N (of NO) and Pt−O (of SO_4^{2-}), however, agree within 0.007 Å with the measured values (Table 2). The calculated O−Pt−N and Pt−N−O angles are 173.0° and 111.5° compared to the measured ones of 171.34(6)°and 117.41(17)°. Thus DFT reproduces the structure also for the platinum complexes with sufficient accuracy, especially for the relevant Pt-NO group, and we can assume that this is true also for the MS. In the MS of **2**, we find a significant elongation in the Pt−O (of NO) bond, which is 2.49 Å, compared to the GS Pt−N distance of 2.08 Å. In **1**, the elongation is from 2.11 Å in GS to 2.59 Å in MS. Also the distance of the *trans*-to-NO ligand is elongated: Pt−O11 (O of SO_4^{2-}) increases from 2.29 to 2.41 Å in **2**, and Pt−O11 (O of NO_3^-) increases from 2.35to 2.58 Å in **1**. The oxygen-bound NO in the MS weakens the Pt−O11 bonds such that the oxygen atoms moves closer to the S of SO_4^{2-} and the N of NO_3^- in **2** and

(32) Enemark, J. H.; Feltham, R. D. *Coord. Chem. Rev.* **1974**, *13*, 339–406.
(33) Peterson, E. S.; Larsen, R. D.; Abbot, E. H. *Inorg. Chem.* **1988**, *27*, 3514–3518.
(34) Bennett, M. A.; Bhargava, S. K.; Bond, A. M.; Bansai, V.; Forsyth, C. M.; Guo, S.-X.; Priver, S. H. *Inorg. Chem.* **2009**, *48*, 2593–2604.
(35) Cormary, B.; Malfant, I.; Valade, L.; Buron-Le Cointe, M.; Toupet, L.; Todorova, T.; Delley, B.; Schaniel, D.; Mockus, N.; Woike, Th.; Fejvarova, K.; Petricek, V.; Dusek, M. *Acta Cryst. B* **2009**, *65*, 612–623.
(36) The X-ray structure of MS was experimentally not obtained because the conversion efficiency of 20% or 26% for the two compounds **1** and **2** is not sufficient to obtain quantitative data as was illustrated in some previous publications (see ref 35). Moreover, it is expected to be rather difficult to detect a change in NO coordination besides the heavy Pt central atom. Given all the spectroscopic and numerical evidence, we could at best obtain some more qualitative information about the MS in these Pt−NO compounds. We would rather search a molecule with higher photoconversion efficiency in order to provide an accurate structure determination of MS.

Table 2. Selected Bond Distances and Angles of **2** and **1** and Comparison to Calculated Structures of **2** and **1**

	2			**1**		
distance (Å)/angle (deg)	exp GS	calc GS	calc MS	exp GS	calc GS	calc MS
Pt−N1	2.0594(16)	2.093	2.087	2.057(6)	2.088	2.079
Pt−N2	2.0535(15)	2.092	2.083	2.057(6)	2.092	2.082
Pt−N3	2.0606(16)	2.079	2.075	2.057(6)	2.084	2.079
Pt−N4	2.0600(15)	2.080	2.078	2.057(6)	2.087	2.074
Pt−N5	2.0807(18)	2.082		2.04(4)	2.110	
N5−O5	1.133(3)	1.165	1.131	1.25(3)	1.175	1.147
Pt−O5			2.491			2.585
Pt−O11	2.2843(14)	2.288	2.412		2.346	2.584
S1−O11	1.4964(14)	1.565	1.551			
S1−O12	1.4627(16)	1.507	1.506			
S1−O13	1.4618(16)	1.506	1.507			
S1−O14	1.4908(16)	1.482	1.489			
N5−Pt−O11	171.34(6)	173.0	175.8		171.4	176.4
Pt−N5−O5	117.41(17)	111.5	125.9	120.1(9)	112.9	125.3
N1−Pt−N3	177.28(6)			180.0		
N2−Pt−N4	177.23(6)			180.0		

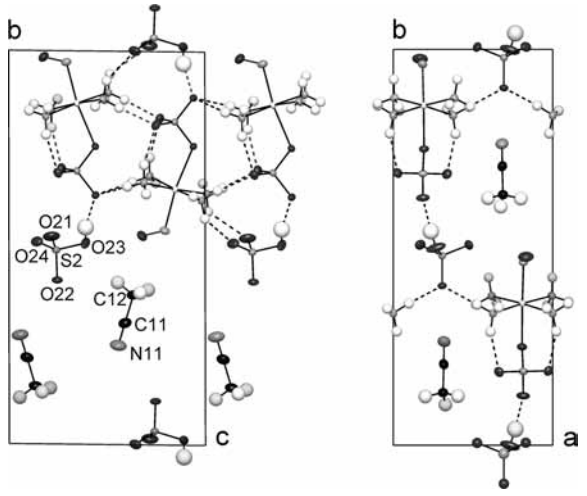

Figure 2. Crystal structure of **2**. Left: view along the *a*-axis. Right: view along the *c*-axis. Atoms are shown from 0 to 0.5 along the *a*- and *c*-axis, respectively, in the same style as for Figure 1. H-bonds are shown as broken lines.

1, respectively. Furthermore, the NO distance and equatorial Pt−N (N of NH_3) distances are slightly shortened. In summary, the NO isomerization leads to bond length changes in the first coordination sphere of the Pt such that the axial distances are elongated, while the equatorial distances are slightly shortened.

Infrared Spectroscopy. Because of the reactivity of the platinum complexes with KBr and CsI, finely ground samples were embedded in nujol and subsequently deposited on a CsI pellet or in AgBr. Embedment in AgBr shifts the ν(NO) vibration by 8 cm^{-1} to higher wavenumbers, while all the other vibrational bands remain unaffected within the resolution of 2 cm^{-1}. Figure 4 shows the infrared spectra of **1** and **2** in the relevant spectral range of 1500−1900 cm^{-1} before and after photoexitation at 660 nm. In the GS, the ν(NO) stretching vibrations are at 1744 cm^{-1} in **1** and at 1714 cm^{-1} in **2**. Thus, there is a strong influence of oxygen on the *trans*-ligand when compared to $[Pt(NH_3)_4Cl(NO)]Cl_2$, where the ν(NO) is at 1673 cm^{-1}. The excitation results in a diminution of the GS ν(NO) band and the appearance of a new band

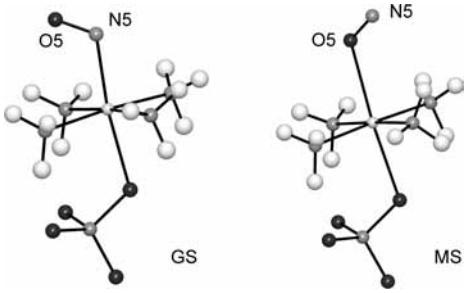

Figure 3. Calculated structure of $[Pt(NH_3)_4(SO_4)NO]^+$ of **2** in GS (left) and MS (right).

at 1815 cm^{-1} for **1** and at 1814 cm^{-1} for **2**. Again, a significant *trans*-effect is observed in comparison to $[Pt(NH_3)_4Cl(NO)]Cl_2$, where the MS ν(NO) band was reported at 1793 cm^{-1}.[12]

For **2**, the first harmonic of the ν(NO) stretching vibration is observed for the GS at 3402 cm^{-1} and at 3602 cm^{-1} for the MS. The anharmonicity is thus almost identical for the GS and MS. Further changes in the IR spectrum are detected in the spectral range of 300−700 cm^{-1}. For **2**, small additional bands appear in the metastable state at 412, 445, 619, and 630 cm^{-1}, which might be redshifted from the respective GS bands at 421, 452, 624, and 632 cm^{-1} that exhibit a decrease in intensity. According to Arndt et al.[37], these bands are attributed to the SO_4^{2-} group. Their small redshift may indicate a decrease in the electron density at the Pt center between the GS and MS. The population of the MS was determined from the decrease in the intensity of the ν(NO) GS stretching vibration. The MS populations amount to 26(2)% for **1** and 20(2)% for **2**. Illumination at 1064 or 532 nm decreases and eventually completely erases the MS population as can be seen from the decrease or vanishing of the ν(NO) stretching vibration of the MS. It indicates a reversible regeneration of the GS from the MS as was described for $[Pt(NH_3)_4Cl(NO)]Cl_2$.[12] Note that the illumination with 1064 nm eventually results also in a complete erasure of MS. Figure 4 shows an

(37) Arndt, A.; Wickleder, M. S. Z. *Anorg. Allg. Chem.* **2008**, *634*, 369–372.

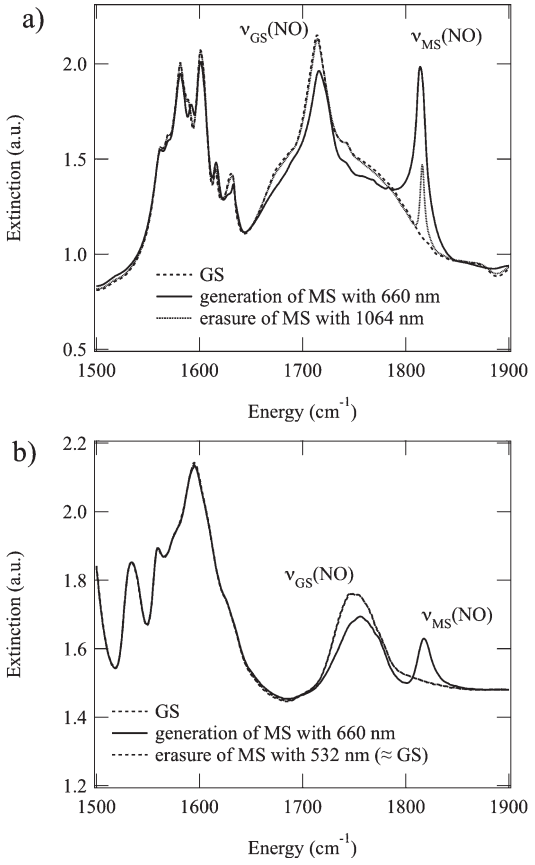

Figure 4. Infrared spectra of $[Pt(NH_3)_4(SO_4)(NO)](HSO_4)(CH_3CN)$ (**2**) in nujol (a) and $[Pt(NH_3)_4(NO_3)(NO)](NO_3)_2$ (**1**) in AgBr (b). After excitation of the GS (dashed line) at 660 nm, the ν(NO) bands of the MS (solid line) are detected at 1815 cm^{-1} **1** and 1814 cm^{-1} **2**. By irradiation with 1064 or 532 nm, the optical depopulation of the MS can be monitored from the decrease in the MS ν(NO) band (dotted curves).

intermediate illumination time in order to clearly demonstrate the decrease of the MS ν(NO) band.

From DFT calculations, the ν(NO) stretching vibrations are obtained at 1736.9 cm^{-1} (**1**) and 1681.1 cm^{-1} (**2**) for the GS and 1884.4 cm^{-1} (**1**) and 1796.1 cm^{-1} (**2**) for the MS (Table 3). Compared to the experimental results, the shift to higher wavenumbers from GS to MS is well-reproduced in the calculations, while the absolute values deviate by $-7/69$ cm^{-1} and $-33/-18$ cm^{-1} for **1** and **2**, respectively.

Differential Scanning Calorimetry. Figure 5 shows the MS thermal decay curve in $[Pt(NH_3)_4(NO_3)(NO)](NO_3)_2$ after irradiation at 660 nm and 90 K. The maximum heat release occurs at 111 K. Using eq 1, the activation energy E_A, frequency factor Z, and total enthalpy of decay could be determined. The significant broadening of the curve points toward the presence of two independent decays with parameters $E_A = 0.18(3)$ eV, $Z = 2 \times 10^6$ s^{-1}, and $H_{tot} = 5.8(2)$ kJ/mol for decay 1 and $E_A = 0.18(3)$ eV, $Z = 6 \times 10^5$ s^{-1}, and $H_{tot} = 7.9(2)$ kJ/mol for decay 2. The error of 0.03 eV in E_A results from the broad decay and the experimental limitation of the temperature range to 90 K. The error in the frequency factor is 1 order of magnitude because of the limited temperature range of the measurement. The total released enthalpy H_{tot} is proportional to the population P and increases with the exposure Q as illustrated in Figure 5b. The envelope of decay 1 and 2 is described with the exponential behavior $H_{tot} = H_{sat}[1 - \exp(-Q/Q_0)]$ with $H_{sat} = 14.4(3)$ kJ/mol and $Q_0 = 21(3)$ J/cm^2. From the population $P = 26\%$ and enthalpy H_{tot}, the energetic position of the MS is derived as $E_{MS} = 0.54(4)$ eV ($H_{tot} = P \times E_{MS}$). Thus, the saddle point between MS and GS amounts to $E_{SP} = 0.72(7)$ eV. Q_0 is a measure of the population velocity. It is comparable to the value found in $[Pt(NH_3)_4Cl(NO)]Cl_2$ but a factor of 100 faster than in other NO compounds.[38] For potential applications, the spectral sensitivity of the MS population is important. In accordance with $[Pt(NH_3)_4Cl(NO)]Cl_2$[12], the maximum for **1** is found at 670 nm, and linkage isomers can be generated in the range 570−800 nm.

Table 3. NO Stretching Vibration Energies of the Ground (GS) and Metastable (MS) States

	experimental (cm^{-1})		calculated[a] (cm^{-1})	
	GS	MS	GS	MS
$[Pt(NH_3)_4(NO_3)(NO)](NO_3)_2$ (**1**)	1744	1815	1736.9	1884.4
$[Pt(NH_3)_4(SO_4)(NO)](HSO_4)(CH_3CN)$ (**2**)	1714	1814	1681.1	1796.1
$[Pt(NH_3)4Cl(NO)]Cl_2$ (ref 12)	1673	1793	1791.1	1875.9

[a] Calculated values are not scaled.

From the DFT calculations, we obtain the ground state potential surface along the reaction coordinate, i.e., the NO rotation, and thus also the three characteristic energies: activation energy E_A, MS energy E_{MS}, and saddle point energy $E_{SP} = E_A + E_{MS}$. These energies are summarized in Table 4 and compared to the experimental values of **1**. The activation energy of **1** is calculated quite accurately, while the MS energy is overestimated by 0.4 eV. Thus, also the saddle point is overestimated by 0.4 eV. However, the observed and calculated saddle point energies are lower than the used photon energy (2.14−1.59 eV), which is a necessary condition for the successful photogeneration of the metastable states. The calculated values for **1** and **2** are rather close with slightly higher values for **2**.

Partial Density of States. In order to clarify which transition is leading to the NO isomerization, we have calculated the partial density of states (pDOS) for **1** and **2** as illustrated in Figure 6 for **2**. The results are in agreement with the earlier obtained pDOS for $[Pt(NH_3)_4(NO)(Cl)]^{2+}$.[12] From the pDOS of Pt and N (of NO) in the GS, it can be seen that the HOMO at −0.60 eV with respect to the Fermi energy E_F is a strongly mixed orbital with Pt(5d) an $\pi^\star$(NO) contributions, a typical signature of π-backbonding of NO with the transition metal. The second highest occupied orbital at −1.67 eV, however, has a stronger Pt(5d) character. The LUMO at 0.50 eV is mainly the $\pi^\star$(NO) orbital with a small admixture of metal d. The orbital at 1.57 eV is of pure metal d character, while the next one at 1.87 eV is again a strongly mixed Pt(5d)-$\pi^\star$(NO) orbital. Taking the energetic differences between the calculated pDOS levels as a measure for comparison with the observed population

(38) Woike, Th.; Krasser, W.; Zöllner, H.; Kirchner, W.; Haussühl, S. *Z. Phys. D* **1993**, *25*, 351–356.

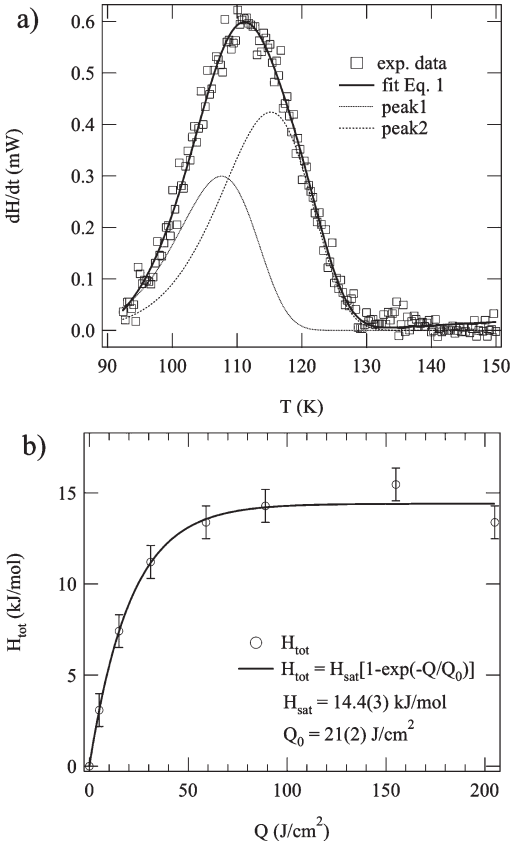

Figure 5. (a) Thermal decay of $[Pt(NH_3)_4(NO_3)(NO)](NO_3)_2$ after light irradiation with 660 nm at 90 K. The solid line is a fit according to eq 1 assuming the presence of two independent decays. Parameter values for the best fit are E_A = 0.18(3) eV, $Z = 2 \times 10^6$ s^{-1} ,and H_{tot} = 5.8(2) for decay 1 and E_A = 0.18(3) eV, $Z = 6 \times 10^5$ s^{-1}, and H_{tot} = 7.9(2) for decay 2. (b) Heat release H_{tot} of the metastable state MS as a function of exposure Q. The population is fast and saturates at 14.4(3) kJ/mol.

Table 4. Activation Energy E_A, MS Energy E_{MS}, and Saddle Point Energy E_{SP}

	Exp. **1**	DFT **1**	DFT **2**
E_A (eV)	0.18(3)	0.154	0.205
E_{MS} (eV)	0.54(4)	0.905	1.026
E_{SP} (eV)	0.72(7)	1.059	1.231

window, we note that the absolute values are underestimated by the calculation. Considering only those orbitals with the highest pDOS around E_F at −0.60 eV, 0.50 eV, 1.57 eV, and 1.87 eV, transition energies of 1.10 eV, 2.17 eV, and 2.47 eV are obtained, respectively. The experimentally determined population window of the MS in the spectral range 580−780 nm corresponds to energies of 2.14−1.59 eV. Thus, the population occurs via the HOMO−LUMO transition Pt(5d) → $\pi^\star$(NO). From the pDOS (Figure 6), it is obvious that the differences between the orbitals around E_F become smaller in the MS. Consequently, all transitions have lower energies, those with the highest pDOS are found at 0.35 and 0.90 eV. Interestingly the $\pi^\star$(NO) orbital (LUMO) of MS has almost no contributions from the metal and is therefore a nearly pure ligand orbital, which is in complete agreement with the findings in $[Pt(NH_3)_4(NO)(Cl)]^{2+}$.[12] All in all, the pDOS shows that the population of the MS occurs via the excitation to the $\pi^\star$(NO) and that in the MS the transitions are redshifted with respect to the GS.

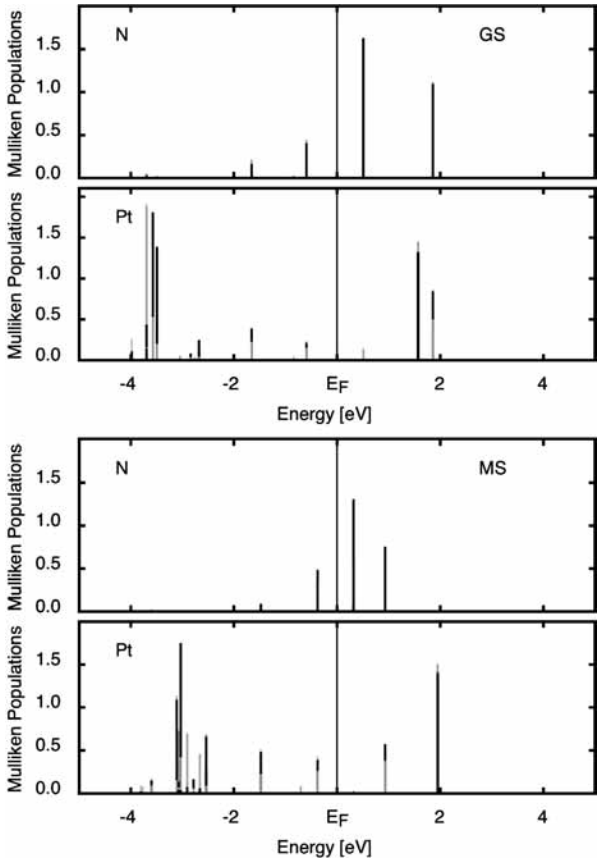

Figure 6. pDOS of GS (top) and MS (bottom) for Pt and N (of NO) in $[Pt(NH_3)_4(SO_4)(NO)]^+$. E_F is the Fermi energy, separating filled and unfilled orbitals. The LUMO is mainly of NO type [$\pi^\star$(NO)], while the HOMO shows significant mixing of Pt(d) and $\pi^\star$(NO). In the MS, the HOMO and LUMO shift to higher and lower energies, respectively, leading to a redshift of the optical transitions with respect to the GS. The occupancies are given as histograms according to the Mulliken population analysis, i.e., electrons per orbital.

Discussion

On the basis of the determination of the structure of $[Pt(NH_3)_4(SO_4)(NO)](HSO_4)(CH_3CN)$, where a Pt−N−O angle of 117.13° was found, we could show that the octahedrally coordinated platinum nitrosyl complexes $[Pt(NH_3)_4X(NO)]$ with X = Cl^-, NO_3^-, and SO_4^{2-} fit into the classification scheme of Enemark and Feltham, which predicts M−N−O angles in the range of 125 ± 10° for $\{MNO\}^8$ complexes. Thus the platinum nitrosyl compounds form a large group of $\{MNO\}^8$ complexes exhibiting photoinduced nitrosyl linkage isomerism. Because to date no structural data were available for these compounds, we can compare the results for $[Pt(NH_3)_4(SO_4)(NO)](HSO_4)(CH_3CN)$ only with the calculated structure of the free $[Pt(NH_3)_4(SO_4)(NO)]^+$ ion.[12] We find that the calculated structure differs by less than 0.06 Å in bond lengths, and deviations in the O−Pt−N and Pt−N−O angles are smaller than 5.6°. Bearing in mind that the calculation was performed on the free cation and that for the used basis set distances are normally overestimated by 0.04 Å,[11] the agreement between calculation and experiment is satisfactory. The calculated structures of the two metastable linkage isomers in **1** and **2** are supposed to be of the same accuracy. Further, the shorter NO bond lengths in **1** and **2** are supported by higher ν(NO) stretching vibrations. These are for **1** and **2** 71 and 42 cm^{-1}, respectively, higher in

energy than in $[Pt(NH_3)_4Cl(NO)]Cl_2$. The exchange of the transligand Cl^- by O^{2-} of SO_4^{2-} or NO_3^- also has consequences for the properties of the metastable state MS. The decay temperature, i.e., the maximum in the heatflow at a heating rate of 4 K/min, is about 10 K lower for the transligand O, which is in accordance with a smaller activation energy of 0.18(3) eV compared to that of 0.27(3) eV found in the Cl compound. Furthermore, the energetic difference of 0.54 eV between the GS and MS for **1** is lower than in the Cl compound with 1.21 eV. Thus, the characteristic parameters of the energy surface along the isomerization reaction coordinate are significantly influenced by changing the *trans*-to-NO ligand. Such a high sensitivity of the *trans*-ligand in $\{MNO\}^8$ complexes is known and was already discussed in detail by Enemark and Feltham.[32] The photogeneration of the linkage isomer in these platinum nitrosyl complexes is initiated via a metal-to-ligand charge transfer from the Pt(5d) to the $\pi^\star$(NO) orbital. As a consequence the Pt−N(O) bond is weakened and the δ(Pt−N−O) mode drives the system to the isomeric configuration.[39] Both in the GS and MS, the NO configuration is staggered with respect to the ammonia ligands and with dihedral angles O−N−Pt−N1 of −130° and 23° for GS and MS, respectively. In all compounds the ν(NO) vibration is shifted to higher wavenumbers in the MS, indicating a shorter NO bond length and a more positive NO ligand as calculated by DFT. Thus, as in the case of $[Pt(NH_3)_4ClNO]Cl_2$, the shift of the NO stretching vibration to higher energies is due to a more positive character of the NO ligand in MS.[12] The population of the MS with light exposure exhibits an exponential behavior needing only a low photon flux of $Q_0 = 21$ J/cm^2 for the GS to MS conversion such that a one-photon excitation is responsible for the triggering of the photoisomerisation.

(39) Schaniel, D.; Woike, Th. *Phys. Chem. Chem. Phys.* **2009**, *11*, 4391–4395.

Conclusions

On the basis of the investigation of octahedrally coordinated platinum nitrosyl compounds, we established a light-induced nitrosyl linkage isomerism as a general property of $\{MNO\}^8$ complexes and thus extend the class of photoswitchable NO complexes beyond the well-known group of $\{MNO\}^6$ compounds. For the $\{MNO\}^8$ compounds, the photogeneration of the metastable linkage isomers occurs via a MLCT transition M(d) $\rightarrow \pi^\star$(NO) in the red spectral range. This represents an advantage with respect to potential pharmaceutical applications compared to the members of the $\{MNO\}^6$ family, whose metastable states are excited in the blue-green spectral range. A further important difference is that two metastable linkage isomers may be formed in the $\{MNO\}^6$ family, while for $\{MNO\}^8$ only one linkage isomer is generated because the NO group is already bent in the ground state configuration. Accordingly, the photogeneration of linkage isomers in $\{MNO\}^8$ complexes is a one-step process and much faster than in the $\{MNO\}^6$ compounds.

Acknowledgment. Financial support by the Swiss National Science Foundation, Deutsche Forschungsgemeinschaft (WO618/8-1, SCHA1550/1-1), and BMBF (FKZ 03X5510) is gratefully acknowledged.

Supporting Information Available: Cif file and selected bond distances and angles for **2** (Table S1). This material is available free of charge via the Internet at http://pubs.acs.org.